

Nonlinear Seismic Response Analysis of Steel–Concrete Composite Frames

Alessandro Zona¹; Michele Barbato²; and Joel P. Conte, M.ASCE³

Abstract: Frame finite-element models permit obtaining, at moderate computational cost, significant information on the dynamic response behavior of steel–concrete composite (SCC) frame structures. As an extension of conventional monolithic beam models, composite beams with deformable shear connection were specifically introduced and adopted for the analysis of SCC beams, in which the flexible shear connection allows development of partial composite action influencing structural deformation and distribution of stresses. The use of beams with deformable shear connection in the analysis of frame structures raises very specific modeling issues, such as the characterization of the cyclic behavior of the deformable shear connection and the assembly of composite beam elements with conventional beam–column elements. In addition, the effects on the dynamic response of SCC frame structures of various factors, such as the shear connection boundary conditions and the mass distribution between the two components of the composite beam, are still not clear and deserve more investigation. The object of this paper is to provide deeper insight into the natural vibration properties and nonlinear seismic response behavior of SCC frame structures and how they are influenced by various modeling assumptions. For this purpose, a materially nonlinear-only finite-element formulation is used for static and dynamic response analyses of steel–concrete frame structures using composite beam elements with deformable shear connection. Realistic uniaxial cyclic constitutive laws are adopted for the steel and concrete materials of the beams and columns and for the shear connection. The resulting finite-element model for a benchmark problem is validated using experimental test results from the literature for quasi-static cyclic tests. The paper then focuses on the numerical simulation, based on various modeling assumptions, of the eigenproperties and seismic response of a realistic two-dimensional five-story two-bay moment resisting frame made of steel columns and SCC beams and designed according to the Eurocode. It is found that the inclusion of the deformability of the shear connection in the finite-element model has a significant effect on the global dynamic response of SCC frame structures. In modeling this type of structures by using frame elements with deformable shear connection, a proper representation of the shear connection boundary conditions for all composite beams is crucial for accurate response simulation.

DOI: 10.1061/(ASCE)0733-9445(2008)134:6(986)

CE Database subject headings: Finite element method; Nonlinear analysis; Seismic effects; Composite structures; Steel; Concrete; Connection.

Introduction

Steel–concrete composite (SCC) structures used in building and bridge construction are subjected to various kinds of dynamic loadings, such as earthquakes, wind, machine-induced vibrations, and traffic loads. Among the various models available for the analysis of composite structures (Spacone and El-Tawil 2004),

frame models allow the obtainment of significant information at reasonable computational cost compared to more sophisticated two-dimensional (plate/shell) and three-dimensional (solid) finite-element (FE) models. Even if frame elements can only account approximately for local effects (e.g., shear lag, local instabilities in the compressed portion of the steel beam, cracking and crushing of concrete), good test-analysis correlation results were obtained by a number of researchers (e.g., Liew et al. 2001; Kim and Engelhardt 2005) for quasi-static tests and global response quantities. As an extension of conventional monolithic beam models, beams with deformable shear connection were specifically introduced and adopted for the analysis of SCC beams. Flexible shear connectors allow development of partial composite action (Viest et al. 1997; Oehlers and Bradford 2000), influencing structural deformation and distribution of stresses under service and ultimate load conditions. Further, the shear connection can be responsible for collapse, e.g., when partial shear connection design is adopted, connectors fail due to limited ductility. Consequently, a composite beam model with deformable shear connection has some important advantages over the common Euler–Bernoulli monolithic beam model, i.e.: (1) it allows a more accurate modeling of the structural behavior; (2) it provides information on the slab–beam interface slip and shear force behavior; (3) it permits to evaluate the effects of the interface slip on stress distribution; and (4) it enables to model damage and failure

¹Assistant Professor, Dept. PROCAM, Univ. of Camerino, Viale della Rimembranza, 63100 Ascoli Piceno, Italy. E-mail: alessandro.zona@unicam.it

²Assistant Professor, Dept. of Civil and Environmental Engineering, Louisiana State Univ. at Baton Rouge, 3531 Patrick F. Taylor Hall, Nicholson Extension, Baton Rouge, LA 70803. E-mail: mbarbato@lsu.edu

³Professor, Dept. of Structural Engineering, Univ. of California at San Diego, 9500 Gilman D., La Jolla, CA 92093-0085 (corresponding author). E-mail: jpconte@ucsd.edu

Note. Associate Editor: Enrico Spacone. Discussion open until November 1, 2008. Separate discussions must be submitted for individual papers. To extend the closing date by one month, a written request must be filed with the ASCE Managing Editor. The manuscript for this paper was submitted for review and possible publication on January 29, 2007; approved on October 8, 2007. This paper is part of the *Journal of Structural Engineering*, Vol. 134, No. 6, June 1, 2008. ©ASCE, ISSN 0733-9445/2008/6-986–997/\$25.00.

of the connectors. Up to date, applications of beam elements with deformable shear connections to the analysis of SCC frames have mainly been limited to quasi-static behavior, with recent work by Dissanayake et al. (2000), Ayoub and Filippou (2000), and Salari and Spacone (2001). On the other hand, there is limited experience on nonlinear dynamic analysis of SCC frames based on beam elements with deformable shear connection (Bursi et al. 2005). In addition, some modeling aspects deserve further investigation. In fact, the use of beams with deformable shear connection in the analysis of frame structures raises very specific modeling issues, such as the characterization of the cyclic behavior of the deformable shear connection and the assembly of composite beam elements with conventional beam-column elements. In addition, the influence of various factors (e.g., shear connection boundary conditions, mass distribution between the two components of the composite beam) on the dynamic response of SCC frame structures needs to be better understood through a systematic parametric study.

The objective of this paper is to provide deeper insight into eigenanalysis and nonlinear dynamic analysis results of SCC structures and how different modeling assumptions affect these results. For this purpose, a materially nonlinear-only FE formulation for static and dynamic analysis of SCC structures using displacement-based locking-free elements with deformable shear connection (Dall'Asta and Zona 2002) is employed. However, the results obtained are not necessarily limited to displacement-based formulations and can be extended to mixed (Dall'Asta and Zona 2004a; Barbato et al. 2007) and force-based elements (Salari and Spacone 2001). Realistic uniaxial cyclic constitutive laws are adopted for the steel and concrete materials of the beams and columns and for the shear connection. The FE simulated cyclic response of a SCC frame structure subassembly is validated through comparison with quasi-static experimental test results (Bursi and Gramola 2000). Then, eigenanalysis and nonlinear dynamic seismic analysis results of two-dimensional moment resisting frames made of steel columns and composite beams are provided. These results and their discussion focus on: (1) the influence of partial composite action on the dynamic nonlinear analysis of SCC frames; (2) the effects of different modeling assumptions related to SCC structures; and (3) modeling recommendations for SCC structures based on their construction details.

Finite-Element Modeling of Steel-Concrete Composite Frames

Beam Model with Deformable Shear Connection

The formulation for two-dimensional beams with deformable shear connection is based on the Newmark et al. (1951) model (Fig. 1), in which (1) the Euler-Bernoulli beam theory (in small deformations) applies to both components of the composite beam; and (2) the deformable shear connection is represented by an interface model with distributed bond allowing interlayer slip and enforcing contact between the steel and concrete components.

A local orthogonal reference frame $\{O; X, Y, Z\}$ is introduced: The Z axis is parallel to the beam axis and the vertical plane YZ is the plane of geometrical and material symmetry of the cross section (Fig. 1). Loads are also assumed symmetric with respect to the YZ plane. The displacement field \mathbf{u} of a material point of the beam is given by

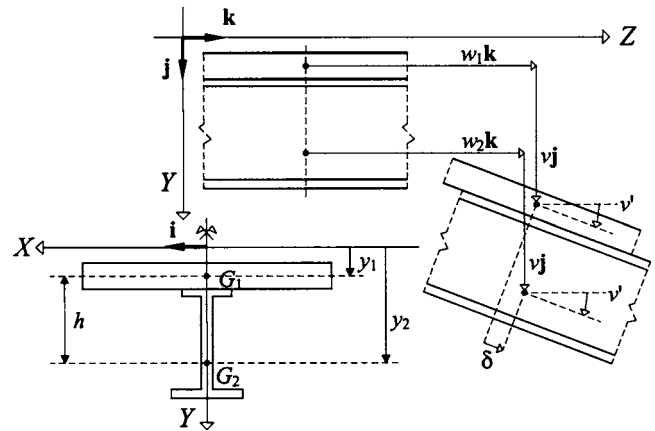


Fig. 1. Kinematics of two-dimensional composite beam model and reference system

$$\mathbf{u}(y, z) = v(z)\mathbf{j} + [w_\alpha(z) + (y_\alpha - y)v'(z)]\mathbf{k} \quad \text{on } A_\alpha \quad (\alpha = 1, 2) \quad (1)$$

where w_α = axial displacement of the reference point of domain A_α , the ordinate of which is y_α ($\alpha=1$: concrete slab, $\alpha=2$: steel beam); v = vertical displacement of the cross section; and \mathbf{j} and \mathbf{k} denote the unit vectors along the Y and Z axes, respectively. It is observed that the transverse displacements and rotations of the slab and of the steel beam are equal due to the enforced contact between the two components. The only nonzero strain components are the axial strain $\varepsilon_{z\alpha}$ and the interface slip δ

$$\varepsilon_{z\alpha}(y, z) = w'_\alpha(z) + (y_\alpha - y)v''(z) \quad \text{on } A_\alpha \quad (\alpha = 1, 2) \quad (2)$$

$$\delta(z) = w_2(z) - w_1(z) + hv'(z) \quad (3)$$

where $h = y_2 - y_1$ = distance between the reference points (G_1 and G_2 in Fig. 1) of the two components. At the locations of the longitudinal reinforcement, Eq. (2) also provides the strain in the reinforcement, due to the assumption of perfect bond between steel and concrete.

Finite-Element Formulations

Different FE formulations were developed based on Newmark's kinematics (Newmark et al. 1951), e.g., displacement-based elements (Daniels and Crisinel 1993; Dall'Asta and Zona 2002), strain-based elements (Cas et al. 2004), two-field (Ayoub and Filippou 2000) and three-field (Dall'Asta and Zona 2004a) mixed elements, and force based elements (Salari and Spacone 2001). The present study makes use of a simple and effective two-dimensional ten nodal degrees-of-freedom (DOFs) displacement-based SCC frame element with deformable shear connection (Dall'Asta and Zona 2002). Eight DOFs are external, i.e., four DOFs per end node (axial displacement, transverse displacement, and rotation of the steel beam and axial displacement of the concrete slab), whereas the remaining two are internal, i.e., axial displacement of the concrete slab and axial displacement of the steel beam (Fig. 2). A useful feature implemented in the frame element adopted is an internal constraint that can be introduced at each SCC beam end independently to enforce zero slip between the steel beam and concrete slab components (Zona et al. 2007). This locking-free element (Dall'Asta and Zona 2004b) was proven to produce accurate results provided that a sufficiently refined mesh is adopted (Dall'Asta and Zona 2004c). The same

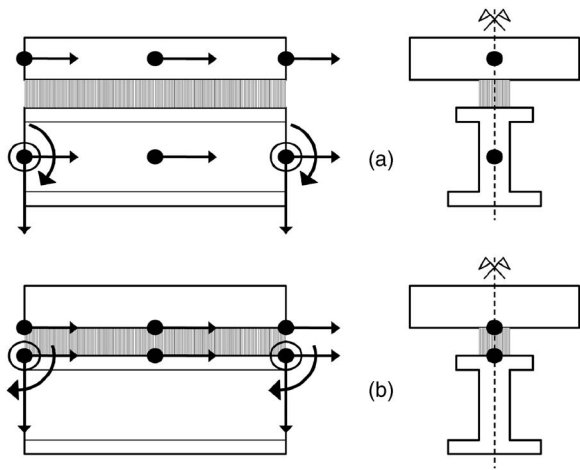


Fig. 2. Degrees of freedom of the 10 DOF composite beam element used: (a) references defined at the beam and slab centroids; (b) references defined at the slab-beam interface

element was employed for finite-element response sensitivity analysis of SCC structures (Zona et al. 2005) under both monotonic and cyclic loading conditions. Results and observations in the present paper are, however, not restricted to the specific finite element used.

Finite-Element Assembly

The assembly of composite beam elements (four DOFs per end node in a two-dimensional formulation) with conventional beam-column elements (three DOFs per end node in a two-dimensional formulation) gives rise to some specific issues (Zona et al. 2007). In this study, different assembly configurations are considered and implemented, corresponding to both common and less common situations in SSC frames (Zona et al. 2007). Rigid beam-to-column connections only are considered. Nevertheless, extension to semirigid connections is possible by introducing special joint elements with prescribed constitutive behavior.

Modeling of Inertia and Damping Properties

In this study, the inertia properties are modeled via translational (horizontal and vertical) masses lumped at the DOFs of the frame elements' external nodes (Zona et al. 2007). Thus, the inertia properties of the finite-element model are independent of the type of finite elements employed, i.e., the same structure mass matrix is obtained using displacement-based, force-based, or mixed-formulation frame elements. Information about damping properties of SCC frame structures inferred from experimental dynamic data is very limited (Bursi and Gramola 2000; Dall'Asta et al. 2005). Friction between steel beams and concrete slabs may be a strong source of structural damping in SCC structures. However, due to lack of quantitative information about this energy dissipating mechanism, preference is given in this study to the well-known and widely used Rayleigh damping model (Chopra 2001), for which it is sufficient to specify a damping ratio at two distinct (modal) frequencies. The Rayleigh damping matrix used herein is proportional to the mass matrix and initial stiffness matrix.

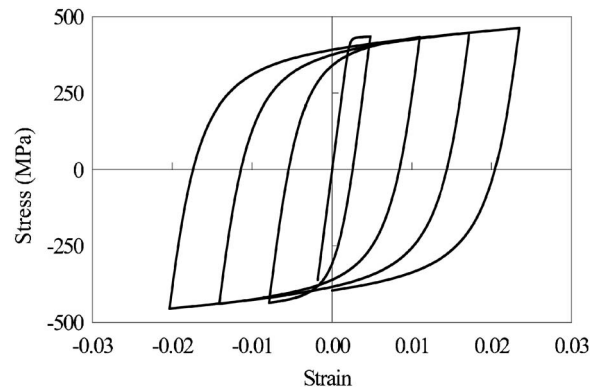


Fig. 3. Menegotto-Pinto material constitutive model for structural steel: typical cyclic stress-strain response

Hysteretic Modeling of Structural Materials and Shear Connection

Steel Constitutive Law

The selected constitutive law for the steel material (reinforcement and beam steel) is the uniaxial Menegotto-Pinto constitutive model (Menegotto and Pinto 1973), a computationally efficient nonlinear smooth law capable to model both kinematic and isotropic hardening (Filippou et al. 1983) and Bauschinger effect, and able to reproduce experimental results very closely. Further details on the model and its numerical implementation can be found in Menegotto and Pinto (1973); Filippou et al. (1983), and Barbato and Conte (2006), where the model is extended for finite-element response sensitivity computation. A typical cyclic response of the steel material model adopted herein for the reinforcement steel is shown in Fig. 3.

Concrete Constitutive Law

The selected constitutive law for the concrete material is a uniaxial cyclic law with monotonic envelope defined by the Popovics-Saenz law (Balan et al. 1997, 2001). The implemented cyclic behavior is characterized by linear unloading-reloading branches with progressively degrading stiffness. After each unloading/reloading sequence, the monotonic envelope is reached again when the absolute value of the largest compressive strain attained so far is surpassed. The concrete in tension follows the same equations and set of loading/unloading/reloading rules as in compression with the same initial stiffness and appropriate values for the other parameters. A complete description of the monotonic and cyclic behavior is given in Zona et al. (2007). A typical cyclic response of the concrete material model adopted in this study for the concrete slabs is shown in Fig. 4.

Shear Connection Constitutive Law

The cyclic constitutive law adopted for the shear connection uses, as monotonic envelope, a function specifically introduced by Ollgaard et al. (1971) for describing the nonlinear behavior of stud shear connectors in SCC beams. The Ollgaard et al. (1971) law is given by the following exponential function which represents the experimentally observed large reduction of stiffness with increasing slip:

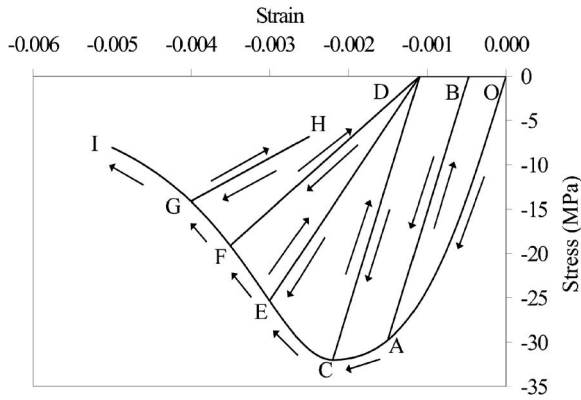


Fig. 4. Hysteretic concrete material model under compression

$$f_s = \begin{cases} f_{s \max}(1 - e^{-\beta\delta})^\alpha & \text{for } \delta \geq 0 \\ -f_{s \max}(1 - e^{-\beta|\delta|})^\alpha & \text{for } \delta < 0 \end{cases} \quad (4)$$

where $f_{s \max}$ =connection strength; δ =slip between the two components of the composite beam; α , β =parameters defining the shape of the curve; and the symbol $|\dots|$ denotes the absolute value of the quantity inside it. Parameters α (with $0 < \alpha \leq 1$) and β control the stiffness (slope of the curve) for small and intermediate (of the order of β^{-1}) values of the slip, respectively. In particular, the curve reaches asymptotically the rigid-plastic model for α approaching zero. Empirical parameters α and β can be identified or calibrated from experimental data. In the present work, the values suggested by Johnson and Molenstra (1991) are adopted, namely $\alpha=0.558$ and $\beta=1 \text{ mm}^{-1}$. As the stiffness at the origin is infinite when $\alpha < 1$, in order to avoid numerical problems, the exponential law is substituted with a linear path (with stiffness k_a) from the origin to an assigned slip δ_a (very small compared to $\delta=\beta^{-1}$). The monotonic envelope description is completed by the definition of an ultimate slip, δ_{ult} . After the maximum absolute value of the slip reaches the ultimate slip, the shear force–slip behavior follows zero-stiffness branches with constant shear force $f_s = \pm \tau_{fr}$, where τ_{fr} =friction (residual shear force).

The implemented cyclic behavior is an idealization of the experimentally observed behavioral trend (e.g., Bursi and Gramola 1999) and its detailed formulation can be found in Zona et al. (2007). Fig. 5 shows a typical cyclic response of the shear force (normalized by $f_{s \max}$)-slip model adopted for all shear connections used in this study. The formulation of a more complex law was beyond the scope of this work. However, despite the simpli-

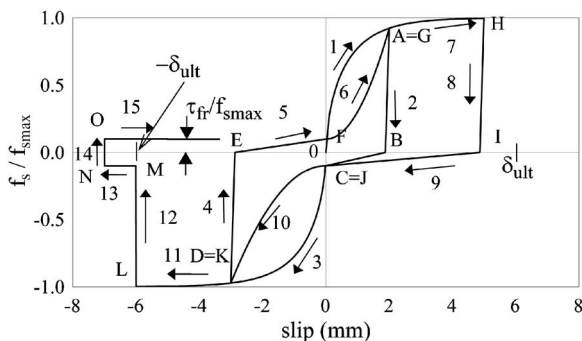


Fig. 5. Hysteretic model of shear connection

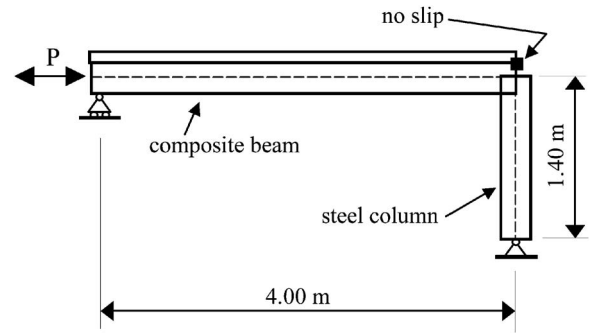


Fig. 6. IPC frame: configuration of test specimen

fications introduced, use of this material model gives good agreement between experimental results and numerical simulations as shown in the model validation section of this paper.

Computer Implementation

The previous formulation for finite-element response analysis using SCC frame elements with deformable shear connection was implemented in FEDEASLab (Filippou and Constantinides 2004), a Matlab (Mathworks 1997) toolbox suitable for linear and non-linear, static and dynamic structural analysis.

Taking advantage of the modularity of FEDEASLab, the existing element, section, and material libraries were extended (i.e., 10 DOF displacement-based composite beam element, composite cross section with symmetrical and nonsymmetrical steel I-beams, new cyclic concrete and shear connection material models) to enable accurate modeling and response simulation of SCC structures. These finite-element libraries can be easily updated and/or extended to reflect the state-of-the-art in modeling such structures.

Model Validation through Test-Analysis Comparison Study

The benchmark problem used to validate the type of numerical model of SCC structures used in this study is a frame sub-assembly tested by Bursi and Gramola (2000) under quasi-static cyclic loading (Fig. 6). The frame sub-assembly, denoted as IPC (intermediate partial connection), is made of a 4.00 m long SCC beam composed of a European IPE300 steel beam and a reinforced concrete slab 1,200 mm wide, and a steel column (European HE360B section). For the composite beam, shear-lag effects are considered in a simplified way reducing the slab width to 820 mm constant along the beam. The reader is referred to Bursi and Gramola (2000) for details regarding the geometry, material properties, and loading history.

The IPC frame is discretized into five 10 DOF composite frame elements of equal length for the beam and one monolithic frame element for the column. The computed load-deflection curve is shown in Fig. 7, where it is compared with the experimental results. It is observed that the analytical and experimental results are in very good agreement, despite the fact that the finite-element model used does not incorporate the effects of local buckling which was experienced by the bottom flange and the web of the steel beam during the push phase of the cyclic loading (last two cycles).

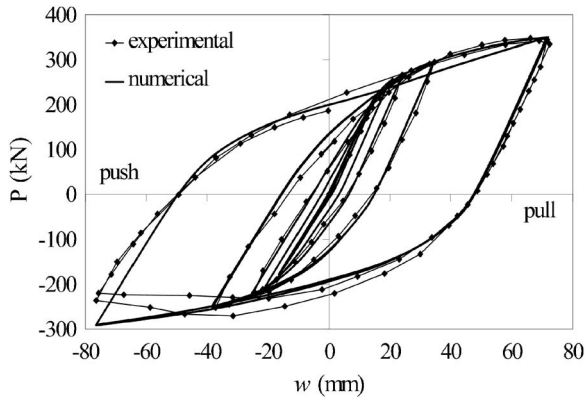


Fig. 7. IPC frame: experimental and numerically simulated load-deflection curves

In a previous study by the writers on finite-element response sensitivity analysis (Zona et al. 2005), the same test structure was analyzed with the only difference that another constitutive law (J_2 plasticity model) was adopted for the steel. By comparing the previous and present results, it is observed that the Menegotto-Pinto model for both the beam steel and the reinforcement steel yields a more accurate approximation of the experimental results.

It is also worth mentioning that the numerical model used in this study for SCC structures was also validated through comparisons with experimental results from tests on continuous beams under monotonic loadings (Zona et al. 2005).

Dynamic Response Simulation of SCC Frame Structures

Description of the SCC Frames Analyzed

The basic testbed SCC frame structure considered in this section is a realistic five-story two-bay moment resisting frame made of steel columns and composite beams (Fig. 8). Each bay has a span of 5.00 m and each story has a height of 3.00 m. The steel columns are made of European HEB300 wide flange beams, while the composite beams are made of steel European IPE270 I-beams connected by means of stud connectors to a 100-mm-thick concrete slab with an effective width estimated at 800 mm (kept constant along the beam), top and bottom reinforcements of 400 mm² and a concrete cover of 30 mm (Fig. 8). The following main material parameters are used: yield stress of column and beam steel=275 MPa, yield stress of reinforcement steel=430 MPa, compressive strength of concrete=33 MPa (see Zona et al. 2007 for all material parameters used). This SCC frame was designed according to Eurocode 4 (CEN 2004a) to resist the static loads (composite cross section self weight=2.36 kN/m, permanent load $G=16$ kN/m, and live load $Q=8$ kN/m with G and Q uniformly distributed along the composite beams) and seismic forces evaluated using response spectrum analysis with peak ground acceleration=0.35 g, Type 1 spectrum of Eurocode 8 (CEN 2004b), modal damping ratio=0.05, soil B, and behavior factor $q=3$.

The shear connection was designed using the plastic approach of Eurocode 4 (CEN 2004a). For the sake of simplicity, the shear connection strength was taken as constant along all composite beams. Three strength levels of the shear connection are considered in this study: (1) the minimum strength for full shear

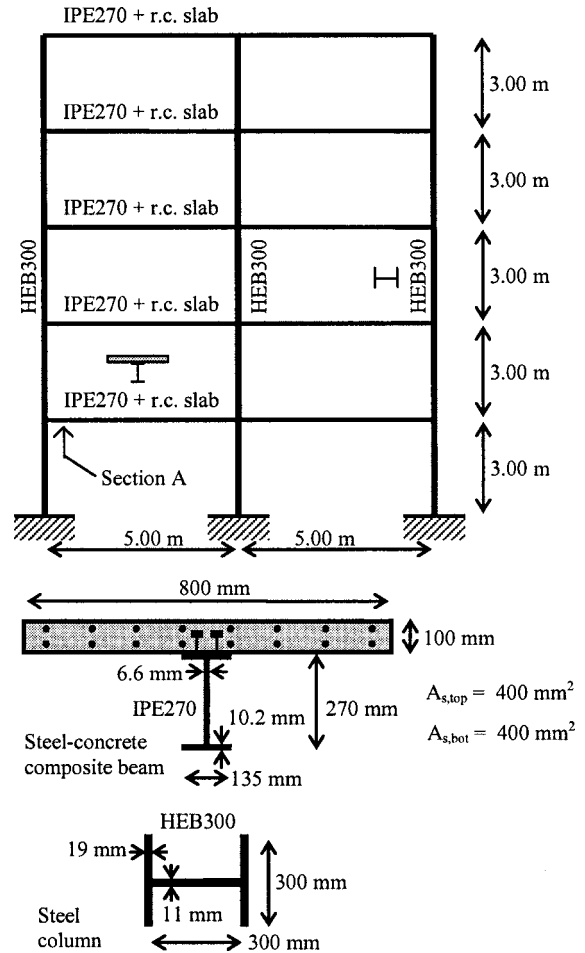


Fig. 8. Testbed structure analyzed: frame configuration and cross-section definition of columns and beams

connection (i.e., the ultimate strength of the composite section is not affected by the shear connectors), denoted as f_{sref} and assumed as basic connection strength ($\psi=f_{smax}/f_{sref}=1$); (2) a partial shear connection (i.e., the ultimate strength of the beam depends on the strength of the shear connection) with $\psi=0.6$; and (3) a full shear connection with a higher degree of interaction ($\psi=1.4$, i.e., less interface slip, than for $\psi=1$). The values of the shear connection constitutive parameters used in this study are reported in Table 1.

For each of the three degrees of shear connection (i.e., shear connection strength levels), several finite-element frame models are used. In all finite-element models used in this study, each beam (between two adjacent columns) is discretized into four 10

Table 1. Shear Connection Parameters Used for the SCC Frame Structures Analyzed

Parameter	$\psi=0.6$	$\psi=1.0$	$\psi=1.4$
f_{smax} (kN/m)	405	675	945
α (—)	0.558	0.558	0.558
β (mm ⁻¹)	1	1	1
δ_u (mm)	8	8	8
τ_{fr} (kN/m)	40.5	67.5	94.5
k_a (MPa)	2,270	3,783	5,296
δ_a (mm)	0.0178	0.0178	0.0178

DOF composite frame elements, and each column (between two adjacent floors) into two conventional displacement-based Euler–Bernoulli (monolithic) frame elements. The finite-element models differ in mass distributions and slip boundary conditions as described in the following.

Three different distributions of the mass equivalent to the permanent load G are considered: (1) mass applied to the slab component only (i.e., permanent load acting directly on the slab, e.g., applied directly on the floor); (2) mass applied to the steel beam component only (i.e., permanent load acting directly on the steel beams, e.g., attached to the ceiling); and (3) mass evenly divided between the slab and steel beam components (i.e., a combination of the two previous cases). The mass equivalent to the self-weight of the SCC beams is distributed between the slab and beam DOFs according to their actual mass. The mass equivalent to the live load Q is assigned entirely to the slab DOFs. In this way, the present study aims at describing and quantifying the influence of different realistic mass distributions on the dynamic properties and seismic response behavior of finite-element frame models which include composite beams with deformable shear connection. It is worth noting that the total mass assigned to each SCC beam (and column) of the FE model is the same in all three cases.

Three different slip boundary conditions are considered for each frame design: (1) slip restrained at every beam–column joint (i.e., the relative slip between slab and steel beam is prevented at the face of every column); (2) slip restrained at the central beam–column joints only (i.e., relative slip between slab and steel beam is prevented at the face of the central column only); and (3) slip free at each joint (i.e., due to sufficient space between columns and slabs, relative slip between slab and steel beam is not prevented). Slip constraints are not applied to the SCC beams at the roof level where the slab is free to slip.

Overall, a set of 27 finite-element models including beams with deformable shear connection was studied. These models are identified with two digits followed by two letters: The digits indicate the degree of shear connection (i.e., 10 for $\psi=1.0$, 06 for $\psi=0.6$, and 14 for $\psi=1.4$); the first letter indicates the mass distribution [i.e., “permanent/dead load” mass evenly distributed between the slab and steel beam components (T), applied to the slab only (S), and applied to the steel beam only (B)]; and the second letter defines the slip boundary condition (i.e., A for slip prevented in all beam–column joints, C for slip prevented in the central beam–column joints only, and N for free slip condition). The FE frame models studied are listed in the first column of Table 2. In addition, a finite-element frame model with conventional Euler–Bernoulli monolithic beams (i.e., equivalent to full shear interaction and full shear connection $\psi=\infty$) was included in this study for comparison purposes. This latter frame model does not require a definition of mass distribution and slip boundary conditions.

Vibration Analysis

A vibration analysis of the SCC frame structure was performed for all three shear connection strength levels based on the different finite-element models defined in the previous section. These eigenanalyses are based on the structure inertia properties previously defined and the tangent stiffness properties of the structural materials after application of the gravity loads (i.e., self-weight, permanent and live loads). The natural period of vibration and modal participating mass ratio (for the horizontal direction) computed for the lowest three vibration modes are reported in Table 2. The lowest three vibration modes are typical lateral

Table 2. Steel–Concrete Composite Five-Story Two-Bay Frames: Vibration Analysis Results

Frame model	Mode 1		Mode 2		Mode 3	
	Period (s)	Mass (%)	Period (s)	Mass (%)	Period (s)	Mass (%)
10TA	0.8729	80.30	0.2903	10.18	0.1584	5.12
10TC	0.9164	80.51	0.2988	10.15	0.1610	5.06
10TN	0.9552	80.30	0.3044	10.14	0.1628	5.06
10SA	0.8730	80.97	0.2902	10.17	0.1584	4.96
10SC	0.9164	80.51	0.2988	10.15	0.1611	5.06
10SN	0.9550	80.28	0.3043	10.14	0.1629	5.06
10BA	0.8728	80.94	0.2903	10.17	0.1584	4.98
10BC	0.9164	80.51	0.2988	10.15	0.1611	5.07
10BN	0.9555	80.32	0.3044	10.14	0.1628	5.05
06TA	0.8809	80.85	0.2929	10.22	0.1593	5.00
06TC	0.9344	80.30	0.3035	10.18	0.1625	5.12
06TN	0.9830	80.04	0.3102	10.15	0.1647	5.11
06SA	0.8811	80.88	0.2929	10.22	0.1593	4.99
06SC	0.9344	80.30	0.3034	10.18	0.1626	5.12
06SN	0.9828	80.02	0.3102	10.15	0.1648	5.11
06BA	0.8807	80.82	0.2930	10.22	0.1593	5.01
06BC	0.9345	80.29	0.3035	10.18	0.1625	5.12
06BN	0.9833	80.06	0.3103	10.15	0.1647	5.10
14TA	0.8692	81.01	0.2889	10.14	0.1580	4.95
14TC	0.9061	80.63	0.2961	10.13	0.1602	5.03
14TN	0.9387	80.45	0.3009	10.13	0.1617	5.02
14SA	0.8693	81.02	0.2889	10.14	0.1580	4.94
14SC	0.9060	80.63	0.2961	10.13	0.1602	5.03
14SN	0.9384	80.44	0.3008	10.13	0.1618	5.03
14BA	0.8691	81.00	0.2890	10.15	0.1580	4.95
14BC	0.9062	80.63	0.2962	10.13	0.1602	5.03
14BN	0.9389	80.47	0.3009	10.13	0.1617	5.02
Monolithic	0.8481	80.18	0.2772	9.79	0.1535	5.06

flexural modes of frame-type structures and their modal participating masses in the horizontal direction account cumulatively for over 95% of the total mass of the structure (between a minimum of 95.03% for the monolithic frame model and a maximum of 96.10% for models 10SA, 14TA, 14SA, and 14BA), whereas less than 1% of the vertical mass of the structure is activated by these three modes. Small variations of the modal periods are observed with changing shear connection stiffness (about 3% decrease in the first mode period from $\psi=0.6$ to $\psi=1.4$): slightly longer periods are obtained for the frame with lower shear connection stiffness due to its increased flexibility (see Table 1 for shear connection initial stiffness values). It could be verified that with increasing shear connection strength (and therefore initial stiffness), the modal periods computed based on the frame model with deformable shear connection tend asymptotically to those obtained from the monolithic frame model (i.e., with rigid shear connection). The results about the effects of the shear connection strength/stiffness on the modal periods obtained in this study are consistent with those presented in Bursi et al. (2005). The results in Table 2 also show that the mass distribution between the slab and steel beam components of the SCC beams has negligible influence on the frame natural periods for the lowest three vibration modes. On the other hand, the slip boundary condition at beam–column joints has a nonnegligible effect on the lowest three natural periods (e.g., difference of 9.4% for the period of the first

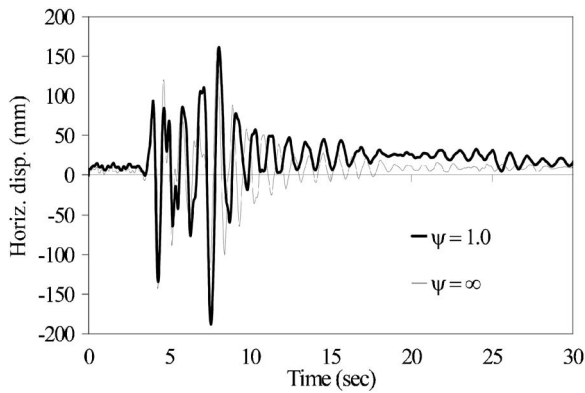


Fig. 9. Horizontal displacement of left column at roof level: effect of deformable shear connection (Northridge seismic input)

mode between a model without slip constraint and a model with slip constraint at each beam–column joint). In terms of modal participating mass ratio, the differences between the various FE models considered are always very small (less than 1%).

Nonlinear Earthquake Response Analysis

After quasi-static application of a vertical distributed load of 26.36 kN/m representing self-weight, permanent and live loads, four nonlinear dynamic analyses were carried out for each frame model considered by using two ground motion accelerograms and two different levels of viscous damping in the structure. The two historic earthquake accelerograms used as base excitation are: (1) the 1994 Northridge Earthquake recorded at the Pacoima Dam Station with a peak ground acceleration (PGA) of 1.585 g, corresponding to a return period of about 180 years (at the recording site); and (2) the 1979 Imperial Valley Earthquake recorded at the Bonds Corner Station with PGA=0.775 g, corresponding to a return period of about 40 years (at the recording site). The two different damping ratios are: (1) $\xi=0.01$; and (2) $\xi=0.05$ at both the first and third vibration modes of the structure (Table 2). The constant average acceleration method, belonging to the family of Newmark- β methods (Chopra 2001), was used as solution method with a constant time step $\Delta t=0.005$ s in all the nonlinear dynamic analyses performed. The corresponding set of nonlinear algebraic equations was solved iteratively using Newton's method

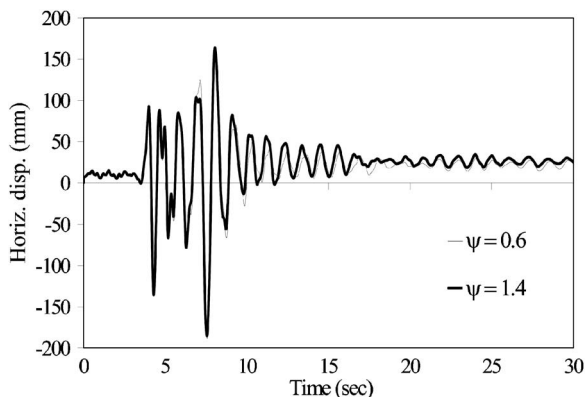


Fig. 10. Horizontal displacement of left column at roof level: effect of connection strength (Northridge seismic input)

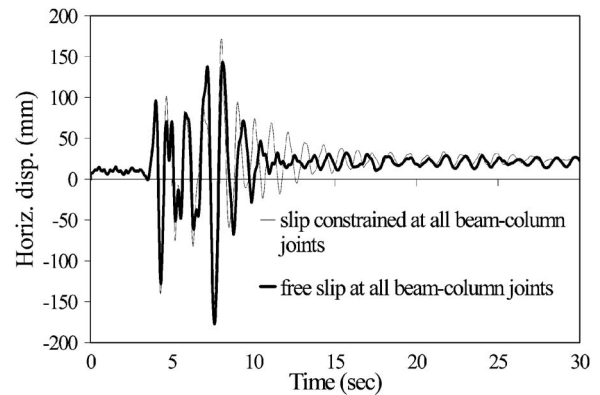


Fig. 11. Horizontal displacement of left column at roof level: effect of slip boundary conditions (Northridge seismic input)

(Chopra 2001). Due to space limitation, in the sequel only selective results are presented. More results can be found in Zona et al. (2007).

Global Response Results

Selected time histories for the horizontal displacement of the left column at the roof level ($z=15$ m) are reported in Figs. 9–12. The results shown in Figs. 9–11 correspond to the Northridge seismic input, whereas Fig. 12 relates to the Imperial Valley seismic input. Unless otherwise specified, the assumed damping ratio at the first and third modes is $\xi=0.05$. The positive and negative peak horizontal roof displacements are reported in Table 3 for selected frame models.

In Fig. 9, the response of the frame model with rigid shear connection ($\psi=\infty$) is compared to the response of the frame model characterized by deformable shear connection with $\psi=1.0$ and slip restrained at the central beam–column nodes only (Frame Model 10TC). The differences in the displacement response between the two models are clearly noticeable. Taking the response of the monolithic frame as reference, the difference in magnitude of the positive and negative peaks is +0.2 and +31.5%, respectively. The maximum absolute difference over the duration of the earthquake is 129.9 mm, and the average absolute difference is 22.5 mm. It is observed that in the case of the monolithic frame, the displacement response oscillates around the static displacement response due to gravity loads only, which is not the case for the frame with deformable shear connection. Fig. 10

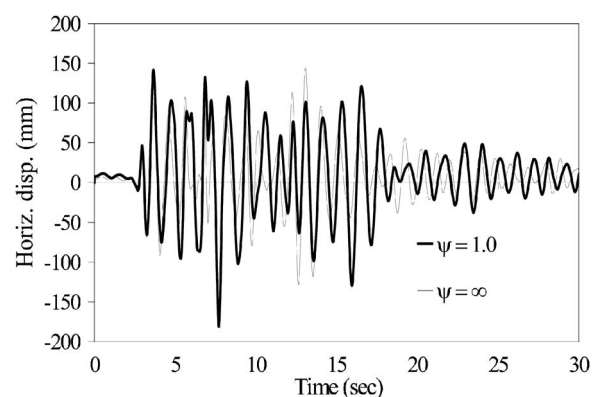


Fig. 12. Horizontal displacement of left column at roof level: effect of deformable shear connection (Imperial Valley seismic input)

Table 3. Positive and Negative Peak Roof Horizontal Displacements and Peak Interstory Drift Ratio for Selected Frame Models (Northridge Seismic Input)

Frame model	Damping ratio (%)	Peak roof displacement (mm)		Peak interstory drift ratio (%)				
		Max	Min	1	2	3	4	5
06TC	5	155.3	-188.7	0.79	1.54	1.68	1.32	1.55
10TC	5	161.3	-188.0	0.78	1.55	1.72	1.31	1.55
10TC	1	170.6	-198.9	0.87	1.56	1.63	1.30	1.81
14TC	5	164.0	-185.2	0.77	1.55	1.71	1.29	1.55
10SC	5	168.3	-183.1	0.75	1.53	1.70	1.28	1.53
10BC	5	161.2	-188.0	0.78	1.55	1.72	1.31	1.55
10TN	5	143.4	-177.0	0.76	1.47	1.54	1.25	1.54
10TA	5	171.8	-167.5	0.77	1.49	1.57	1.25	1.57
Monolithic	5	161.0	-143.0	0.66	1.22	1.30	1.16	1.25

shows the effect of the connection strength by comparing the cases $\psi=1.4$ and $\psi=0.6$. Both models (Frames 14TC and 06TC) have slip restrained at the central beam-column nodes only and same mass distribution. Taking the case $\psi=1.4$ as reference, the difference in magnitude of the positive and negative peaks is -5.3 and $+1.9\%$, respectively. The maximum absolute difference over the duration of the earthquake is 48.6 mm, and the average absolute difference is 8.8 mm.

Fig. 11 shows the effect of slip boundary conditions on the roof horizontal displacement by considering two extreme cases, namely slip (1) restrained (Frame Model 10TA); and (2) unrestrained (Frame Model 10TN) at all beam-column joints. Taking Frame Model 10TA as reference, the difference in magnitude of the positive and negative peaks is -16.5 and $+5.7\%$, respectively. The maximum absolute difference over the duration of the earthquake is 95.8 mm, and the average absolute difference is 14.1 mm. The effect of the mass distribution observed by comparing the roof displacement responses of Models 10SC and 10BC is small (Zona et al. 2007) with maximum difference of -4.2% taking Frame Model 10SC as reference (Table 3). A larger effect due to structural damping is observed by comparing the roof displacement responses obtained from Frame Model 10TC for $\xi=0.05$ and $\xi=0.01$, respectively. Taking the case $\xi=0.05$ as reference, the difference in magnitude of the positive and negative peaks is $+5.8$ and $+16.6\%$, respectively (Table 3). To evaluate the influence of a different seismic excitation, Fig. 12 presents the roof displacement responses for the same models (monolithic frame and Frame 10TC) as in Fig. 9 subjected to the (less intense)

Imperial Valley Earthquake. Again, the difference in the two model responses is evident (difference in magnitude of the positive and negative peaks $=-1.5$ and $+40.8\%$, respectively, maximum absolute difference $=108.6$ mm, average absolute difference $=51.2$ mm). These results are consistent with those of Bursi et al. (2005) who also investigated the effect of partial composite action on the seismic response of SCC structures. However, Bursi et al. (2005) did not investigate the effects of slip boundary conditions and mass distributions, and assumed a level of viscous damping dependent on the degree of shear connection (i.e., the weaker the connection, the higher the damping). Therefore, their studies did not allow to quantify the individual effects of the level of damping and the degree of shear connection.

The peak interstory drifts (defined as the percentage ratio d_r/h , where d_r =peak interstory drift and h =story height) for selected frame models subjected to the Northridge Earthquake are reported in Table 3. Using Frame Model 10TC with $\xi=0.05$ as reference, it is observed that for a given story the differences in peak interstory drift obtained from the various models vary in the range $[-10.5\%, +16.8\%]$, which is of width similar to the difference in peak interstory drift predicted based on the frame model with monolithic beams (maximum difference of -24.4%). Table 4 reports the positive and negative peak values of the interstory shears obtained from the response history analyses (for the Northridge Earthquake input) of the same frame models as in Table 3. Fig. 13 represents graphically the interstory drift and shear demands for the frame model with monolithic beams and Frame Model 10TC (with $\xi=0.05$) subjected to the Northridge

Table 4. Positive and Negative Peak Interstory Shears for Selected Frame Models (Northridge Seismic Input)

Frame model	Damping ratio (%)	Peak interstory shear (kN)									
		1	2	3	4	5					
06TC	5	408.1	-459.0	340.9	-367.1	316.1	-375.1	262.0	-349.4	302.5	-279.8
10TC	5	403.3	-469.7	323.9	-392.6	332.5	-393.0	269.3	-353.0	310.3	-289.1
10TC	1	472.9	-585.6	405.0	-406.5	359.2	-407.3	287.3	-425.5	388.6	-306.0
14TC	5	398.4	-475.3	332.5	-404.5	342.4	-401.0	273.6	-354.0	313.1	-294.3
10SC	5	388.1	-463.7	324.8	-395.5	339.7	-393.3	255.6	-346.5	305.9	-295.2
10BC	5	403.8	-469.4	323.8	-392.0	332.5	-392.9	269.0	-353.3	309.7	-288.4
10TN	5	380.2	-452.9	336.2	-342.3	292.4	-339.7	262.3	-338.5	300.4	-265.8
10TA	5	442.2	-485.3	374.6	-429.8	380.5	-415.1	283.7	-366.6	324.5	-314.9
Monolithic	5	501.1	-451.3	438.0	-444.9	441.1	-446.3	409.4	-366.7	452.1	-361.4

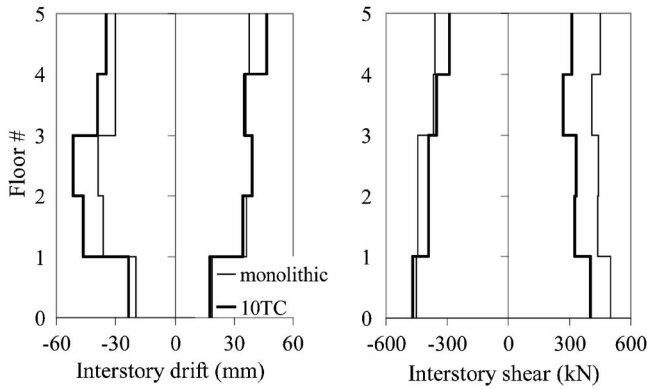


Fig. 13. Interstory drift and shear demand: effect of deformable shear connection (Northridge seismic input)

Earthquake input. Thus, response simulation of SCC frame structures modeled using frame elements with deformable shear connection (as compared to monolithic frame elements) leads to: (1) larger seismic demand in terms of floor displacements and interstory drifts; and (2) lower seismic demand in terms of interstory shears. As expected, the interstory shear demand increases with the overall stiffness of the frame model (as measured by the fundamental period of the model). It is also important to note that the viscous damping ratio (in the range $\xi=0.01-0.05$) is the modeling parameter (among the ones considered in this study) to which the maximum (over all stories) peak interstory shear is most sensitive. This conclusion is also corroborated by other analysis results (based on other combinations of modeling parameters/assumptions and the Imperial Valley Earthquake input) not presented here due to space limitation.

Local Response Results

This section presents a selection of local response results of interest. Fig. 14 shows a comparison of the bending moment–curvature responses (for the Northridge Earthquake) at Beam Section A defined in Fig. 8, obtained from the frame model with monolithic beams and Frame Model 10TC (both with $\xi=0.05$). The bending moment is computed at the steel–concrete interface level in the composite beam cross section. A significant difference is observed in the results obtained from the frame model with monolithic beams and frame models using beams with deformable shear connection. Fig. 15 shows the same comparison,

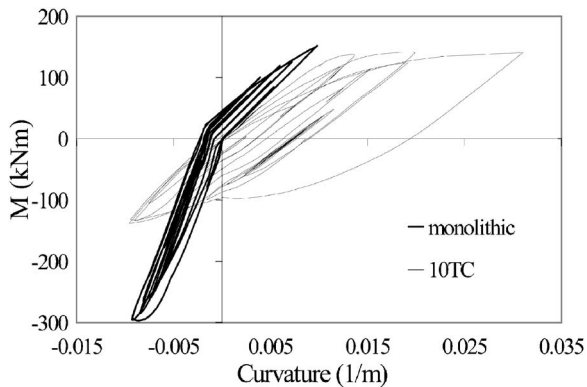


Fig. 14. Moment–curvature response at beam section A (see Fig. 8): effect of deformable shear connection (Northridge seismic input)

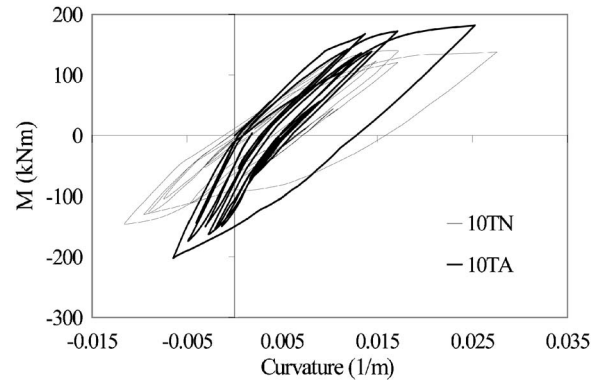


Fig. 15. Moment–curvature response at beam section A (see Fig. 8): effect of slip boundary conditions (Northridge seismic input)

but between Frame Models 10TA and 10TN, to study the effect of different slip boundary conditions. It is seen that the presence of slip constraints (at all beam–column joints) has the effect of increasing significantly the bending moment demand, simultaneously reducing the curvature demand. It was verified that these local response results for the considered SCC frame with deformable shear connection converge to their counterparts for the corresponding frame with monolithic beams as the strength (and therefore stiffness) of the shear connection increases (i.e., increasing ψ).

Interlayer slip response envelopes (over the entire response histories for the Northridge Earthquake) along the SCC beam axes are shown for Floors 1–4 in Figs. 16–18. These response envelope results are not given for the roof beams, as the latter have no slip constraints unlike the other beams (except for Frame Model 10TN) leading to significantly larger interlayer slip, especially for Frame Model 10TA. The effect of different slip boundary conditions on the interlayer slip response envelopes is observed by comparing the results presented in Fig. 16 (Frame Model 10TA with slip restrained at all beam–column joints), Fig. 17 (Frame 10TN with free slip everywhere), and Fig. 18 (Frame 10TC with slip restrained at the beam–column joints along the central column). These results correspond to a degree of shear connection $\psi=1.0$, damping level $\xi=0.05$, and the Northridge seismic input. As expected, the magnitude and spatial distribution along the beams of the interlayer slip are strongly influenced by the slip boundary conditions. It is interesting to observe that peaks in the slip distribution along the beams occur

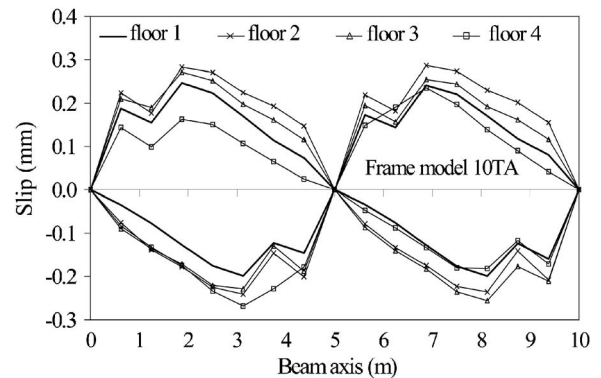


Fig. 16. Interlayer slip response envelopes along SCC beam axes for Frame Model 10TA (Northridge seismic input)

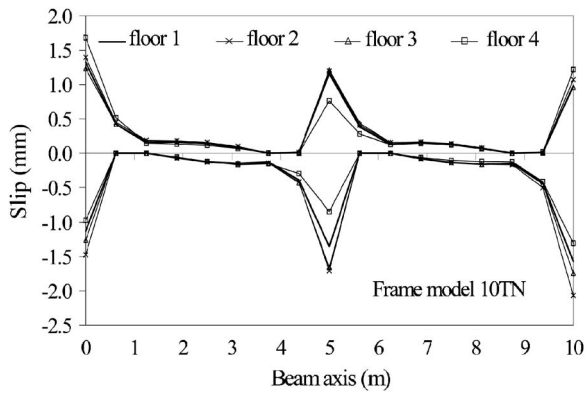


Fig. 17. Interlayer slip response envelopes along SCC beam axes for Frame Model 10TN (Northridge seismic input)

at locations where a concentrated bending moment is transferred (from a column) to the steel beam and concurrently the slab is free to slip. This is due to the enforcement of the contact between the steel beam and concrete slab components of the SCC beams, which results into an equal curvature constraint between these two components. Thus, the application of a concentrated bending moment to the steel beam of a SCC beam produces locally a curvature increase in both the steel beam and concrete slab, which in turn causes a large strain discontinuity [i.e., large slip gradient, see Eq. (3)] at the steel–concrete interface. The effect of the degree of shear connection on the interlayer slip response is shown in Fig. 19, where the slip envelopes for the SCC beam along the second floor are given for Models 06TC, 10TC, and 14TC. These results correspond to the same slip boundary conditions, i.e., slip restrained at the beam–column joints along the central column. For these three cases, the peak slip (over all floors) is 2.82 mm ($\psi=0.6$), 2.46 mm ($\psi=1.0$), and 2.14 mm ($\psi=1.4$), i.e., the peak slips for the weaker and stronger connection are about 15% more and 13% less, respectively, than the peak slip of the intermediate connection strength.

Similar results (not shown here due to space limitations) for local response and how they are affected by various modeling assumptions/parameters were obtained for the lower level of damping ($\xi=0.01$) and the other earthquake input (Imperial Valley Earthquake). It was also found that different mass distribu-

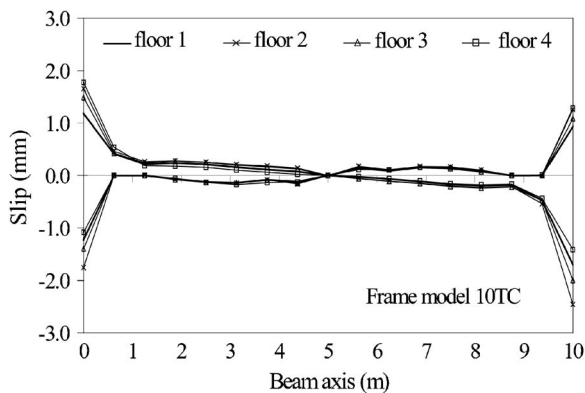


Fig. 18. Interlayer slip response envelopes along SCC beam axes for Frame Model 10TC (Northridge seismic input)

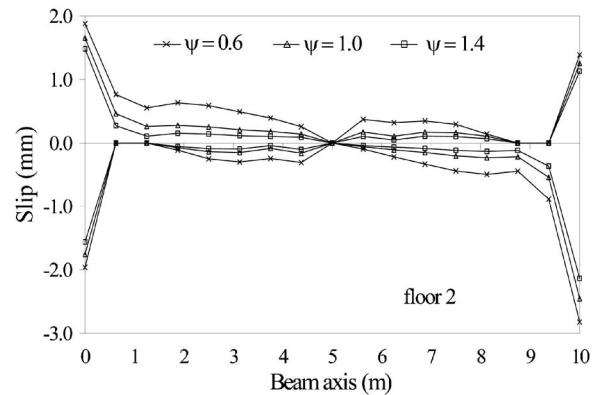


Fig. 19. Interlayer slip response envelopes of SCC beam along the second floor for Frame Models 06TC, 10TC, and 14TC (Northridge seismic input)

tions between the two components of the SCC beams have a negligible effect on the local response results considered here (Zona et al. 2007).

Conclusions

This paper focuses on vibration analysis and dynamic nonlinear analysis of steel-concrete composite (SCC) frame structures through finite-element analysis using frame elements with deformable shear connection. Realistic hysteretic constitutive models are adopted for the concrete, reinforcement steel, beam steel, and shear connection. The response prediction capability of this type of finite-element models of SCC frames is validated using experimental results available in the literature for composite frame subassemblages subjected to cyclic loading.

In order to gain better insight into the natural vibration characteristics and nonlinear seismic response behavior of SCC frame structures and how corresponding numerical predictions are affected by various modeling assumptions and parameters, a realistic five-story two-bay moment resisting frame made of steel columns and composite beams was adopted as basic SCC frame testbed structure. This structure was designed for three degrees of shear connection (partial, full with minimum strength requirement, and full with higher strength). For each of these designs, parametric finite-element studies were performed by varying modeling parameters (within a reasonable range) and assumptions, namely (1) interlayer slip boundary condition; (2) mass distribution between the concrete slab and steel beam components of the composite beams; and (3) level of viscous damping used to model the various sources of energy dissipation not related to material hysteretic behavior. The seismic response was simulated for two different historic earthquakes corresponding to two different hazard levels.

The following remarks are made by comparing simulation results obtained from frame models with monolithic beams and frame models with beams including deformable shear connections. The shear connection deformability has a significant effect on the lower natural frequencies and global seismic response of the SCC frames analyzed, i.e., increase of modal periods, floor displacements, interstory drifts, and decrease of interstory shear demand. These effects are amplified when slip constraints are not present at any beam–column joints, and for low values of shear connection strength (degree of shear connection) and hence con-

nection stiffness. It was found that the mass distribution between slab and steel beam has a minor influence on the natural frequencies and global dynamic response behavior of the SCC frames considered. Thus, a proper representation of the slip boundary conditions for all composite beams is crucial for accurate response simulation.

In addition to the study of the effect of partial composite action in the global response prediction, a frame model with deformable shear connection also provides useful information on the response of the shear connection itself. This local response prediction, obtained at a relatively low additional computational cost (as compared to frame models with monolithic beams), allows evaluation of the shear connection behavior under dynamic/seismic load. The results show that (1) both the magnitude and spatial distribution along the beams of the interlayer slip are strongly influenced by the slip boundary conditions; (2) the degree of shear connection influences only the magnitude of the interlayer slip; and (3) the mass distribution between the concrete slab and steel beam components has negligible effects on the shear connection response. In terms of recommendations for finite-element modeling of SCC frame structures, the following remarks are made based on the results obtained in this study:

1. Use of frame finite elements with deformable shear connection is essential to predict accurately the structural response of SCC frame structures and necessary to simulate the response of the shear connection in terms of interface slip and shear force.
2. Proper representation of the slip boundary conditions of the shear connection at beam-column joints is crucial for accurate response prediction, both at the global and local levels. At beam-column joints where the column passes through the concrete slab, slip between steel beam and concrete slab is prevented and a slip constraint should be applied in the finite-element model. In other situations (e.g., at roof level, at external columns), unless appropriate construction details are employed, interface slip cannot be completely avoided and thus slip constraints should not be applied.
3. The degree of interaction of the composite beams affects significantly the overall stiffness and displacement/deformation demand. Thus, the stiffness properties (correlated to the strength) of the shear connections must be specified accurately. The connection model used in this study allows to define explicitly both the initial stiffness and strength of the shear connections.
4. The amount of viscous damping used in finite-element models of SCC structures has a significant effect on their simulated seismic response. Only scarce information is available on appropriate values of viscous damping ratios to be used in modeling SCC frame structures. The two values used in this study (i.e., 0.01 and 0.05) can be viewed as reasonable lower and upper bounds when energy dissipation due to material hysteretic behavior is already modeled explicitly.
5. The mass distribution between the steel beam and concrete slab components of composite beams is of minor importance with respect to the simulated response (both at the global and local levels) of SCC frame structures. Thus, for ordinary cases, detailed information on mass distribution between beam and slab is not required.

Acknowledgments

Partial supports of this research by the National Science Foundation under Grant No. CMS-0010112, the Pacific Earthquake

Engineering Research (PEER) Center through the Earthquake Engineering Research Centers Program of the National Science Foundation under Award No. EEC-9701568, and the National Center for Supercomputing Applications (NCSA) under Grant No. MSS040022N involving utilization of the IBM P690 computers are gratefully acknowledged. The writers would like to thank Professor Enrico Spacone at the University of Chieti-Pescara in Italy for his support during this study. The third writer would also like to acknowledge partial support of this research by a Senior Fulbright Research Scholarship at the University of Chieti-Pescara.

References

- Ayoub, A., and Filippou, F. C. (2000). "Mixed formulation of nonlinear steel-concrete composite beam element." *J. Struct. Eng.*, 126(3), 371–381.
- Balan, T. A., Filippou, F. C., and Popov, E. P. (1997). "Constitutive model for 3D cyclic analysis of concrete structures." *J. Eng. Mech.*, 123(2), 143–153.
- Balan, T. A., Spacone, E., and Kwon, M. (2001). "A 3D hypoplastic model for cyclic analysis of concrete structures." *Eng. Struct.*, 23(4), 333–342.
- Barbato, M., and Conte, J. P. (2006). "Finite-element structural response sensitivity and reliability analyses using smooth versus non-smooth material constitutive models." *Int. J. Reliability and Safety*, 1(1–2), 3–39.
- Barbato, M., Zona, A., and Conte, J. P. (2007). "Finite-element response sensitivity analysis using three-field mixed formulation: General theory and application to frame structures." *Int. J. Numer. Methods Eng.*, 69(1) 114–161.
- Bursi, O. S., and Gramola, G. (1999). "Behaviour of headed stud shear connectors under low-cycle high amplitude displacements." *Mater. Struct.*, 32(4), 290–297.
- Bursi, O. S., and Gramola, G. (2000). "Behaviour of composite substructures with full and partial shear connection under quasi-static cyclic and pseudo-dynamic displacements." *Mater. Struct.*, 33(3), 154–163.
- Bursi, O. S., Sun, F. F., and Postal, S. (2005). "Nonlinear analysis of steel-concrete composite frames with full and partial shear connection subjected to seismic loads." *J. Constr. Steel Res.*, 61(1), 67–92.
- Cas, B., Bratina, S., Saje, M., and Planinc, I. (2004). "Nonlinear analysis of composite steel-concrete beams with incomplete interaction." *Steel Compos. Struct.*, 4(6), 489–507.
- Chopra, A. K. (2001). *Dynamics of structures: Theory and applications to earthquake engineering*, 2nd Ed., Prentice-Hall, Englewood Cliffs, N.J.
- Comité Européen de Normalization (CEN). (2004a). "Eurocode 4: Design of composite steel and concrete structures—Part 1.1: General—General rules and rules for buildings." *EN 1994-1-1*, Brussels.
- Comité Européen de Normalization (CEN). (2004b). "Eurocode 8: Design of structures for earthquake resistance—Part 1: General rules, seismic actions and rules for buildings." *EN 1998-1-1*, Brussels.
- Dall'Asta, A., Dezi, L., Giacchetti, R., Leoni, G., and Ragni, L. (2005). "Dynamic response of composite frames with rubber-based dissipating devices: Experimental tests." *Proc., 4th Int. Conf. on Advances in Steel Structures*, Z. Y. Shen, G. Q. Li, and S. L. Chan, eds., Elsevier, Oxford, U.K., 741–746.
- Dall'Asta, A., and Zona, A. (2002). "Nonlinear analysis of composite beams by a displacement approach." *Comput. Struct.*, 80(27–30), 2217–2228.
- Dall'Asta, A., and Zona, A. (2004a). "Three-field mixed formulation for the nonlinear analysis of composite beams with deformable shear connection." *Finite Elem. Anal. Design*, 40(4), 425–448.
- Dall'Asta, A., and Zona, A. (2004b). "Slip locking in finite elements for composite beams with deformable shear connection." *Finite Elem.*

- Anal. Design*, 40(13–14), 1907–1930.
- Dall'Asta, A., and Zona, A. (2004c). "Comparison and validation of displacement and mixed elements for the nonlinear analysis of continuous composite beams." *Comput. Struct.*, 82(23–26) 2117–2130.
- Daniels, B. J., and Crisinel, M. (1993). "Composite slab behaviour and strength analysis. Part I: Calculation procedure." *J. Struct. Eng.*, 119(1), 16–35.
- Dissanayake, U. I., Burgess, I. W., and Davison, J. B. (2000). "Modelling of plane composite frames in unpropped construction." *Eng. Struct.*, 22(4), 287–303.
- Filippou, F. C., and Constantinides, M. (2004). "FEDEASLab getting started guide and simulation examples." *Technical Rep. No. NEESgrid-2004-22*, www.ce.berkeley.edu/~filippou/FEDEASLab/NEES-grid-TR22.pdf (Jan. 2007).
- Filippou, F. C., Popov, E. P., and Bertero, V. V. (1983). "Effects on bond deterioration on hysteretic behavior of reinforced concrete joints." *Rep. No. EERC 83-19*, Earthquake Engineering Research Center, Univ. of California, Berkeley, Calif.
- Johnson, R. P., and Molenstra, N. (1991). "Partial shear connection in composite beams for buildings." *Proc. Inst. of Civ. Eng. (UK)*, 91(2), 679–704.
- Kim, K. D., and Engelhardt, M. D. (2005). "Composite beam element for nonlinear seismic analysis of steel frames." *J. Struct. Eng.*, 131(5), 715–724.
- Liew, J. Y. R., Chen, H., and Shanmugam, N. E. (2001). "Inelastic analysis of steel frames with composite beams." *J. Struct. Eng.*, 127(2), 194–202.
- MathWorks Inc. (1997). *Matlab—High performance numeric computation and visualization software, user's guide*, The MathWorks Inc., Natick, Mass.
- Menegotto, M., and Pinto, P. E. (1973). "Method of analysis for cyclically loaded reinforced concrete plane frames including changes in geometry and nonelastic behavior of elements under combined normal force and bending." *Proc., IABSE Symp. on Resistance and Ultimate Deformability of Structures Acted on by Well-Defined Repeated Loads*, International Association for Bridge and Structural Engineering, Zurich, Switzerland, 112–123.
- Newmark, N. M., Siess, C. P., and Viest, I. M. (1951). "Tests and analysis of composite beams with incomplete interaction." *Proc. Soc. Exp. Stress Anal.*, 9(1), 75–92.
- Oehlers, D. J., and Bradford, M. A. (2000). *Elementary behaviour of composite steel and concrete structural members*, Butterworth-Heinemann, London.
- Ollgaard, J. G., Slutter, R. G., and Fisher, J. W. (1971). "Shear strength of stud connectors in lightweight and normal weight concrete." *Eng. J.*, 2, 55–64.
- Salari, M. R., and Spacone, E. (2001). "Analysis of steel-concrete composite frames with bond-slip." *J. Struct. Eng.*, 127(11), 1243–1250.
- Spacone, E., and El-Tawil, S. (2004). "Nonlinear analysis of steel-concrete composite structures: State of the art." *J. Struct. Eng.*, 130(2), 159–168.
- Viest, I. M., Colaco, J. P., Furlong, R. W., Griffs, L. G., Leon, R. T., and Wyllie, L. A. (1997). *Composite construction design for buildings*, McGraw-Hill, New York.
- Zona, A., Barbato, M., and Conte, J. P. (2005). "Finite-element response sensitivity analysis of steel-concrete composite beams with deformable shear connection." *J. Eng. Mech.*, 131(11), 1126–1139.
- Zona, A., Barbato, M., and Conte, J. P. (2007). "Nonlinear seismic response analysis of steel-concrete composite frames." *Rep. No. SSRP-07/11*, Dept. of Structural Engineering, Univ. of California, San Diego.